Engineering Failure Analysis 42 (2014) 38–44

Contents lists available at ScienceDirect

Engineering Failure Analysis

journal homepage: www.elsevier.com/locate/engfailanal

Failure analysis of 316L stainless steel crucible by molten fluoride salt interaction with clay bonded silicon carbide

Robert S. Sellers, Mark H. Anderson, Kumar Sridharan *, Todd R. Allen

Department of Engineering Physics, University of Wisconsin-Madison, 1500 Engineering Dr., Madison, WI 53711, USA

ARTICLE INFO

Article history:
Received 8 August 2012
Received in revised form 23 February 2014
Accepted 9 March 2014
Available online 19 March 2014

Keywords:
Chemical analysis
Hot corrosion
Failures
Microanalysis

ABSTRACT

Detailed investigation of a recently failed static corrosion test involving molten eutectic LiF–NaF–KF salt at 850 °C contained in 316L stainless steel crucibles shows that a single sealed crucible leaked molten salt into the electric furnace due to mechanical failure, causing a chemical reaction between the molten salt and the clay bonded silicon carbide insulation used in the furnace. As a result, corrosive vapors of Na_2SiF_6, K_2SiF_6, SiF_3, and F_2, were formed. These vapors reacted with the stainless steel crucibles and lead to the formation of a porous corrosion crust and the eventual catastrophic structural failure of all nine sealed 316L stainless steel crucibles.

1. Introduction

Fluoride salt mixtures are used in industry as high temperature heat transfer fluids, heat treatment baths and media for electroplating [1]. Recently, research has been directed towards using eutectic fluorides as potential primary and secondary reactor coolants for Generation IV nuclear power plants [1–11]. One mixture, 46.5%LiF–11.5%NaF–42%KF (mol%), commonly referred to as FLiNaK, has generated interest due to its advantageous thermo physical properties including relatively low melting point, high thermal conductivity, high specific heat, low viscosity and high boiling point [1,10].

Structural material compatibility is a concern when using fluoride salts at high temperatures. Typically, stainless steels derive their passive nature from a thin oxide film formation at the surface. However, in the presence of FLiNaK, these oxide films are unstable due to the reduction-oxidation (redox) reaction of fluorine ions with oxide scales of Cr, Al or Si [12]. Traditional fluoride salt corrosion of structural materials involves the depletion of chromium at the surface of the exposed material [13–16].

High temperature systems containing fluoride salts commonly require substantial insulation to prevent accidental freezing and to minimize trace heat. However, little effort has been directed towards studying the interaction between fluoride salts and common insulation materials, which can occur in the event of a leak or failure. Therefore, very little is known how insulation introduced to a fluoride salt environment will impact the corrosion of structural materials.

In the present study, the failure of a 316L stainless steel crucible containing FLiNaK molten salt and subsequent interaction with furnace materials will be examined. Visual inspection, scanning electron microscopy techniques (SEM–EDS), and X-ray diffraction (XRD) analysis are carried out to identify the root cause of the system failure and understand the molten salt interactions with the furnace insulation material. However, it bears emphasizing that this study is a retroactive failure

* Corresponding author. Address: 1500 Engineering Dr., Rm. 815, Madison, WI 53711, USA. Tel.: +1 608 263 4789; fax: +1 608 263 7451.
E-mail address: kumar@engr.wisc.edu (K. Sridharan).

http://dx.doi.org/10.1016/j.engfailanal.2014.03.007
1350-6307/

investigation in a test environment where some details are unknown. As such, the best is made of the limited quantitative information available combined with relevant literature.

2. Experimental

The original purpose of the experiment was to create a controlled test environment to study the static corrosion characteristics of clean molten FLiNaK on structural materials. The test consisted of nine crucibles constructed of 316L stainless steel tube with wall thickness approximately 3 mm, welded shut on both ends and containing 512g FLiNaK. Installed in each crucible were several alloy test coupons upon which analysis would be performed at the conclusion of the test.

Salt preparation, crucible filling and final welding was performed in a dry argon atmosphere glove box. At the testing temperature of 850 °C, each sealed crucible would become pressurized to an extent corresponding to the initial quantity of argon contained in each crucible. Previous static corrosion tests have been fabricated and tested in the same manner with a successful outcome [14,16].

3. Corrosion characterization and discussion

3.1. Visual observation

Fig. 1 shows visual characteristics of the crucibles and the high temperature electric box furnace after the termination of the test. A close up comparison of a corroded crucible and a crucible prior to testing is shown in Fig. 2. The scale formation is porous and brittle with shiny metallic sections and areas of green, white, purple, and red residue. The crucible interiors show relatively thin predominately red scale formations. Two steel sheathed type K thermocouples were used to monitor the internal temperature. Both were nonoperational due to heavy corrosion at the conclusions of the 1000 h test. The alumina sheathed type S control thermocouple remained operational the entire time and appeared unaffected. Throughout the duration of the test, the furnace was held at slight positive pressure with nitrogen cover gas making oxygen ingress unlikely.

The furnace base plate, constructed of 1 mm sized particles of silicon carbide held in a clay matrix, showed extensive attack. The clay matrix is composed of minerals containing O, Si and Al. A cross section of the base plate can be seen in Fig. 3 where affected areas are discolored black. The black damaged region is accompanied by light swelling, indicative of vapor formation.

Upon inspection, it appears that the set of nine static test crucibles failed by several different mechanisms. Some crucibles exhibit circumferential cracking, shown in Fig. 4. Localized outward plastic deformation near the cracks indicates that they are stress induced. These stress ruptures are likely created by lowered crucible structural integrity caused by outward corrosion combined with internal pressurization of the argon cover gas contained within the sealed crucible. It has been shown that a structurally sound crucible is able to contain this minor pressurization, therefore this failure mode depends on the presence of corrosive vapor so stress induced cracking cannot be the method by which FLiNaK was first released into the furnace [16]. One crucible shown in Fig. 5 has a prominent failure point located at a weld joint. All failure modes considered, a faulty weld with a pinhole leak is likely the reason why FLiNaK initially escaped into the furnace.

3.2. SEM/EDS and XRD characterization

To understand the nature of the test failure, samples of corrosion crust from the top of a crucible were investigated using scanning electron microscopy (SEM) equipped with energy dispersive X-ray spectroscopy (EDS). Pieces taken from the top of the corroded crucibles display a variety of morphologies. Fig. 6 shows jagged, rough sections identified in Table 1 to be rich in O, Si, K and Fe dispersed among smoother sections composed primarily of O, K and Cr. Mixed within the jagged sections are

Fig. 1. Photograph of crucibles at the conclusion of the 1000 h static test.

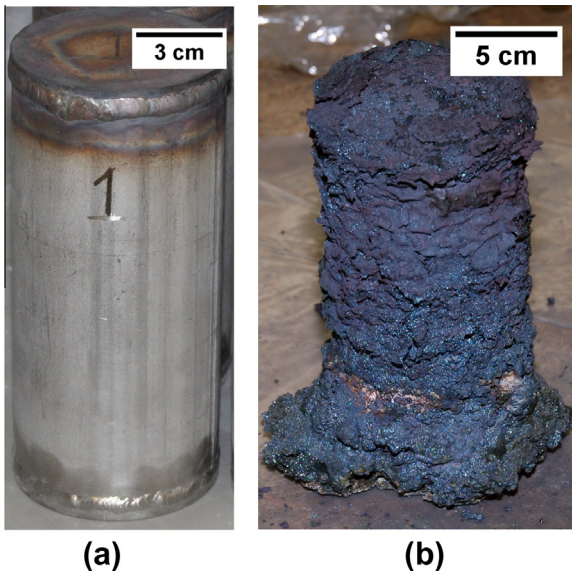

Fig. 2. A comparison of a crucible (a) before corrosion test and (b) after corrosion test. There was substantial height and radial growth of the scale.

Fig. 3. Cross section of the clay bonded SiC base plate used in the high temperature furnace. Affected areas are discolored black with some associated swelling.

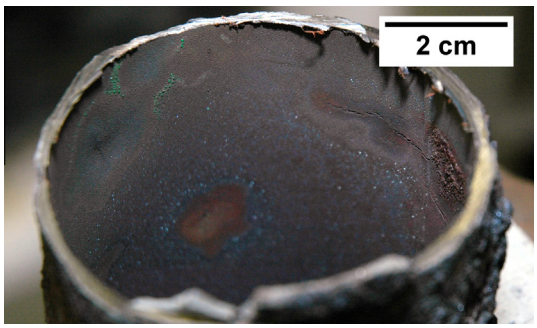

Fig. 4. Circumferentially aligned stress cracking on the interior of one of the static test crucibles.

points containing only Fe and O, identified as α-Fe_3O_3 (hematite). Cross section SEM/EDS maps and point scans of the crucible wall are shown in Fig. 7 and Table 2 Depletion of iron and chromium along grain boundaries starting at the crucible exterior and moving radially inwards appears to be the main mode of attack. EDS point scans identify the F, Na, K rich compound existing between the grains as K_2NaCrF_6. XRD analysis of green substance present on the interior of the corroded crucibles provides positive identification of the presence of K_2NaCrF_6 in the test system as shown in Fig. 8. The distinct emerald green color and X-ray pattern is consistent with the description of K_2NaCrF_6 synthesized and characterized by Knox and Mitchell [17].

EDS detection of F, Si, Na and K on the top of the corroded crucible suggests the elements existed in vapor form at the testing temperature of 850 °C. These elements are abundant in the system in either solid or liquid phases in the form of clay bonded SiC and molten FLiNaK salt, respectively. Thus, a reaction occurred between the molten salt and furnace insulation materials which lead to the creation of a corrosive vapor. Large quantities of oxygen were detected on the surface crust.

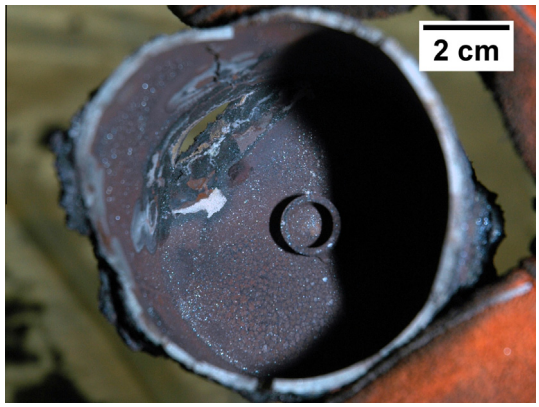

Fig. 5. Point of failure located on the bottom weld.

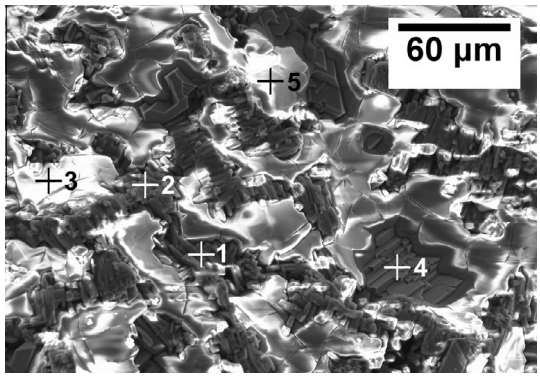

Fig. 6. SEM micrograph of scale topology.

Table 1
EDS elemental distribution of scale topology.

Number	EDS chemical composition (at.%)					
	O	Al	Si	K	Cr	Fe
1	58.8	2.2	14.0	12.2	0.5	12.2
2	61.4	2.2	13.0	11.0	0.7	11.4
3	67.5	–	–	21.3	10.6	0.5
4	63.3	–	–	1.0	0.6	33.6
5	63.6	–	–	23.3	11.9	1.1

However, oxygen was not present in large quantities in the system at testing conditions, so was likely introduced at the conclusion of the test when the furnace was opened to atmospheric air. Prior to opening the furnace, the temperature was allowed to cool to approximately 250 °C. This could be a sufficiently high temperature to allow some surface oxidation. Further evidence that oxygen reactions were an isolated surface phenomenon is backed up by the lack of detected oxygen in the SEM/EDS cross sectional images of Fig. 7. Therefore, oxygen was not a contributing factor to the failure of the system.

3.3. Discussion

The test failure was likely initiated by a pinhole leak in a single crucible which allowed FLiNaK to escape and react with the clay bonded silicon carbide furnace base plate. The reaction taking place at 850 °C created corrosive vapors of SiF_3, F_2, Na_2SiF_6, and K_2SiF_6, evident through the migration of initially solid or liquid phase elements (Si, F, Na, K) to the exterior of the 316L stainless steel crucibles and to the surface of steel sheathed thermocouples positioned above the crucible set. Investigation of the identity of these destructive vapors is pertinent, although precise identification of the vapors is made difficult by the complicated nature of the failure and subsequent material interaction.

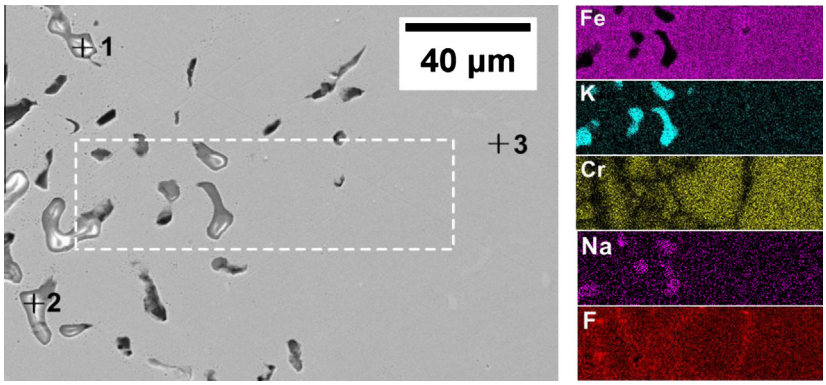

Fig. 7. SEM micrograph of a crucible wall cross section with the corresponding EDS map elemental distribution.

Table 2
Point scan elemental distribution of a crucible wall cross section.

Number	EDS chemical composition (at.%)									Identification
	F	Na	Si	K	Cr	Mn	Fe	Ni	Mo	
1	62.7	9.8	–	17.5	9.0	–	0.8	–	–	K_2NaCrF_6
2	59.2	10.2	–	19.7	10.1	–	0.8	–	–	K_2NaCrF_6
3	–	–	1.4	–	18.0	1.9	67.6	10.3	0.9	γ (Fe,Ni)

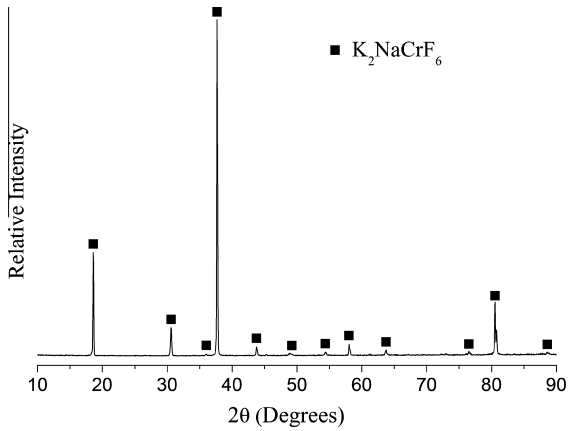

Fig. 8. X-ray diffraction pattern of green material recovered from the crucible.

Fluoride salts are a convenient medium for electrodeposition, especially in silicon containing systems [4,5,18,19]. In addition, fluoride salts and silicon compounds have been studied as pack cementation materials for the creation of steel coatings [6,7,20,21]. Therefore, the test results for the aforementioned studies are useful in understanding the present work because similarities in materials.

Of particular significance is a study performed by Elwell [5] where silicon was electrodeposited from solutions of SiO_2 and fluoride salt eutectics at high temperatures. In measuring the solubility of SiO_2 in various fluoride salt mixtures, it was noted that several mixtures produced volatile products at high temperatures. In particular, Na_2SiF_6 condensate was identified through XRD in NaF/MgF_2 and NaF/CaF_2 melts held at 1000–1100 °C. Additionally, K_2SiF_6 was thought to evaporate from mixtures containing KF. It is possible that these two vapors were created in the present study through an interaction of KF and NaF with the clay bonded silicon carbide furnace materials.

Fukumoto et al. [7] described a pack cementation process for creating a silicon rich layer in SUS430 and SUS304. Silicon containing diffusion layer was observed in alloy samples covered in Si, SiO2 and NaF powder mixture held for 24 h at 950 °C. Considering the similarities between SUS304 and 316L stainless steel, it is likely such a process could occur in the present study. Silicon transport into the metallic matrix can occur by Eqs. (1)–(3).

$$12NaF(g) + 15SiO_2(s) + Si(s) = 6Na_2Si_2O_5(l) + 4SiF_3(g) \quad (1)$$

$$SiF_3(g) + M = Si(s) + MF_3(g) \quad (2)$$

$$SiF_3(g) + 2M = 2Si(s) + 2MF_2(g) + F_2(g) \quad (3)$$

$$M : \text{Metal element}(Fe, Cr, Ni)$$

Initially, a silicon fluoride vapor is formed between silicon oxide and sodium fluoride (Eq. (1)) and proceeds to comes in contact with the alloy surface (Eq. (2)). Continuing the reaction, metal fluoride compounds along with fluorine gas is formed and solid silicon is liberated at the alloy surface (Eq. (3)) and is able to diffuse into the steel, leading to the formation of the Si rich layer. In the Fukumoto paper [7], the chemical reactions were explained using thermodynamic calculations as well as XRD identification of the $6Na_2Si_2O_5$.

A similar process likely occurred in the present study due to the abundant supply of NaF, SiO_2 and Si contained in the box furnace system at high temperatures. Eq. (4) is hypothesized as an explanation for the formation of K_2NaCrF_6 taking into account the process described by Fukumoto along with the K_2SiF_6/Na_2SiF_6 vapors shown to have been created in similar experimental systems. Such a reaction would also provide additional silicon fluoride vapor near the alloy surface to continue the fluorination process described by Fukumoto in Eqs. (2) and (3).

$$2Na_2SiF_6(g) + 4K_2SiF_6(g) + 4Cr(s) + 3F_2(g) = 4K_2NaCrF_6(s) + 6SiF_3(g) \quad (4)$$

The formation of metallic fluorine compounds described by Fukumoto is consistent with the attack seen in the EDS cross sectional image of Fig. 7, where depletion of chromium and iron can be observed. Previous work has shown that chromium and iron are the most thermodynamically favored alloying constituents for fluorine attack in a 316L stainless steel system [14]. In addition, it has been shown that Iron (II) Fluoride can sublimate at temperatures as low as 690 °C [22]. Such a sublimation process explains the distinct iron voids in Fig. 7 as well as the porous structure of the corrosion crust whereby Iron (II) fluorine vapor pockets would exert pressure on surrounding material, causing expansion and eventual release of FeF_2 vapor. Combining the Fukumoto silicon fluoride diffusion theory with the sublimation of FeF_2 and the synergistic effects of the K_2SiF_6/Na_2SiF_6 vapors over hundreds of hours, it can be seen how this processes would create a porous corrosion crust that compromises the structural integrity of the stainless steel tube.

4. Conclusion

Visual inspection, SEM/EDS examination, and XRD analysis were carried out to investigate the failure of a 316L stainless steel molten fluoride salt containing system in a high temperature box furnace held at 850 °C for 1000 h. It was found that FLiNaK molten salt escaped through a pinhole leak in a single static test crucible and reacted with the clay bonded silicon carbide base plate installed in the box furnace. Vapors of SiF_3, Na_2SiF_6, and K_2SiF_6 were formed and subsequently attacked the 316L system through a fluorination process described by Fukumoto and Elwell. It is hypothesized that this process contributed to the creation of K_2NaCrF_6 identified by XRD as well as the sublimation of FeF_2. These combined effects extended over hundreds of hours created a porous corrosion crust which caused the remaining static test crucibles to become structurally unsound. The compromised crucibles released additional FLiNaK contents which continued the vapor corrosion process.

5. Recommendations

Considering the large quantity of insulation typically found in systems containing heated molten salt and the destructive nature of the resulting corrosive vapors, some recommendations to further understand reaction mechanisms and minimize test failures are as follows:

1. Construct a stainless steel boat or perform the test in a retort furnace so leaked salt will come into contact with metallic components only. Such interactions are fairly well understood and vapors will not be created.
2. Minimize internal pressurization of corrosion testing vessels through hot finish welding, vacuum sealing or atmospheric vented apparatus.
3. Verify weld integrity through X-ray analysis.
4. A campaign of theoretical, electrochemical and experiential studies is required to truly understand molten fluoride salt insulation interaction. The work presented here is hindered by the need to retroactively construct a narrative using quantitative clues as opposed to a narrowly defined bottom-up approach.

Acknowledgements

The authors are very grateful to the Department of Energy of the United States of America for funding support under Grant No. DOE-FC07-05ID14675 and DOE-FC07-07ID14826. This research utilized NSF-supported shared facilities at the University of Wisconsin.

References

[1] Holcomb DE, Cetiner SM. An overview of liquid-fluoride-salt heat transport systems. ORNL/TM-2010/156; 2010.
[2] United States Department of Energy. A technology roadmap for generation IV nuclear energy systems. GIF-002-00; 2002.
[3] Flanagan GF, Holcomb DE, Cetiner SM. FHR generic design criteria. ORNL/TM-2012/226; 2012.
[4] Stern KH, McCollum ME. Electrodeposition of silicon from molten salts. Thin Solid Films 1985;124:129–34.
[5] Elwell D. Electrowinning of silicon from solutions of silica in alkali metal fluoride/alkaline earth fluoride eutectics. Solar Energy Mater 1981;5:205–10.
[6] Kim MT, Jung JS. Codeposition of Al and Si onto a low carbon steel using silicon dioxide and aluminum and its hot temperature oxidation properties. Surf Coat Technol 2002;161:218–23.
[7] Fukumoto M, Tachikawame C, Matsuzaka Y, Hara M. Formation of Si diffusion layer on stainless steels and their high temperature corrosion resistance in molten salt. Corros Sci 2012;56:105–13.
[8] Ambrosek J, Anderson M, Sridharan K, Allen T. Current status of knowledge of the fluoride salt (FLiNaK) heat transfer. Nucl Technol 2009;165:166–73.
[9] Ozeryanaya IN. Corrosion of metals by molten salts in heat-treatment processes. Met Sci Heat Treat 1985;3:184–8.
[10] Williams DF. Assessment of candidate molten salt coolants for the NGNP/NHI heat-transfer loop. ORNL/TM-2006/69; 2006.
[11] Williams D, Toth L, Clarno K. Assessment of candidate molten salt coolants for the advanced high-temperature reactor (AHTR). ORNL/TM-2006/12; 2006.
[12] Williams DF, Toth LM. Chemical considerations for the selection of the coolant for the advanced high-temperature reactor. ORNL/GEN4/LTR-05-011; 2005.
[13] Olson LC. Materials corrosion in molten LiF-NaF-KF salt [Ph.D. dissertation]. University of Wisconsin-Madison; 2009.
[14] Olson LC, Ambrosek JW, Sridharan K, Anderson MH, Allen TR. Materials corrosion in molten LiF–NaF–KF salt. J. Fluorine Chem. 2009;130:67–73.
[15] Olson LC, Ambrosek JW, Cao G, Sridharan K, Anderson MH, Allen TR. Molten salts for nuclear cogeneration. Adv Mater Sci Environ Nucl Technol 2010;222:145–56.
[16] Cheng WJ, Sellers RS, Anderson MH, Sridharan K, Wang C, Allen TR. Zirconium effect on the corrosion behavior of 316L stainless steel alloy and Hastelloy-N superalloy in molten fluoride salt. Nucl Technol 2013;183:248–59.
[17] Knox K, Mitchell DW. The preparation and structure of K2NaCrF6, K2NaFeF6 and K2NaGaF6. J Inorg Nucl Chem 1961;21:253–8.
[18] Bieber AL, Massot L, Gibilaro M, Cassayre L, Chamelot P, Taxil P. Fluoroacidity evaluation in molten salts. Electrochim Acta 2011;56:5022–7.
[19] Bieber AL, Massot L, Gibilaro M, Cassayre L, Taxil P, Chamelot P. Silicon electrodeposition in molten fluorides. Electrochim Acta 2012;62:282–9.
[20] Hsu H, Tsai W. High temperature corrosion behavior of siliconized 310 stainless steel. Mater Chem Phys 2000;64:147–55.
[21] Tatemoto K, Ono Y, Suzuki RO. Silicide coating on refractory metals in molten salt. J Phys Chem Solids 2005;66:526–9.
[22] Kent R, Margrave JL. Mass spectometric at high temperatures. VIII. The sublimation pressure of iron(II) fluoride. J Am Chem Soc 1965;87:4754–6.